Anisotropic Adsorption of Molecular Assemblies on Crystalline Surfaces

Jaehun Chun,[†] Je-Luen Li,[‡] Roberto Car,[‡] Ilhan A. Aksay,[†] and Dudley A. Saville*,[†]

Departments of Chemical Engineering and Chemistry, Princeton University, Princeton, New Jersey 08544-5263

Orientational order of surfactant micelles and proteins on crystalline templates has been observed but, given that the template unit cell is significantly smaller than the characteristic size of the adsorbate, this order cannot be attributed to lattice epitaxy. We interpret the template-directed orientation of rodlike molecular assemblies as arising from anisotropic van der Waals interactions between the assembly and crystalline surfaces where the anisotropic van der Waals interaction is calculated using the Lifshitz methodology. Provided the assembly is sufficiently large, substrate anisotropy provides a torque that overcomes rotational Brownian motion near the surface. The probability of a particular orientation is computed by solving a Smoluchowski equation that describes the balance between van der Waals and Brownian torques. Torque aligns both micelles and protein fibrils; the interaction energy is minimized when the assembly lies perpendicular to a symmetry axis of a crystalline substrate. Theoretical predictions agree with experiments for both hemi-cylindrical micelles and protein fibrils adsorbed on graphite.

Introduction

Surfactants in aqueous solution form micelles due, in part, to the limited solubility of their hydrocarbon tails. Spherical, cylindrical, bilayer, and bicontinuous structures occur, depending on the characteristics of the molecules and their concentrations.[1] Atomic force microscope (AFM) studies show that, when these micelles adsorb on crystalline templates, they display an orientational order dictated by the crystal structure of the template.[2−7] Similar observations are made with proteins on highly ordered pyrolytic graphite (HOPG)[8,9] although the same proteins in solution display a "wavy" fibrillar structure.[10] The fact that adsorption produces well-defined configurations suggests that patterned structures can be organized at the nanometer length scale. Molecular assemblies are especially appealing as templates for building composite structures because the length scale is small, typically a few nanometers, and controlled by molecular architecture.

Orientational relationships appear insensitive to the composition of the adsorbate. For example, Aksay et al.[4] showed that cationic, hemi-cylindrical micelles of cetyltrimethylammonium chloride (CTAC) adsorb on HOPG in patterns with (three) preferred directions (Figure 1). While the micelles align perpendicular to the symmetry axes of graphite, individual surfactant molecules on the surface are oriented parallel to the axes. Identical orientational relations are observed when de novo synthetic proteins adsorb onto HOPG (Figure 2).[8,9] Not surprisingly, the directionality is absent on amorphous carbon (Figure 2B).[9]

Anisotropic adsorption of molecular assemblies has not been limited to micellar and protein systems. Organic thin films grown by vapor deposition of planar molecules commonly display orientational order on crystalline templates.[11−15] In addition, simple alkane molecules such as $C_{19}H_{40}$ and $C_{50}H_{102}$ show the alignment and domain formation on crystallite

* Corresponding author. E-mail: dsaville@princeton.edu. Telephone: 609-258-4585. Fax: 609-258-6835.
† Department of Chemical Engineering.
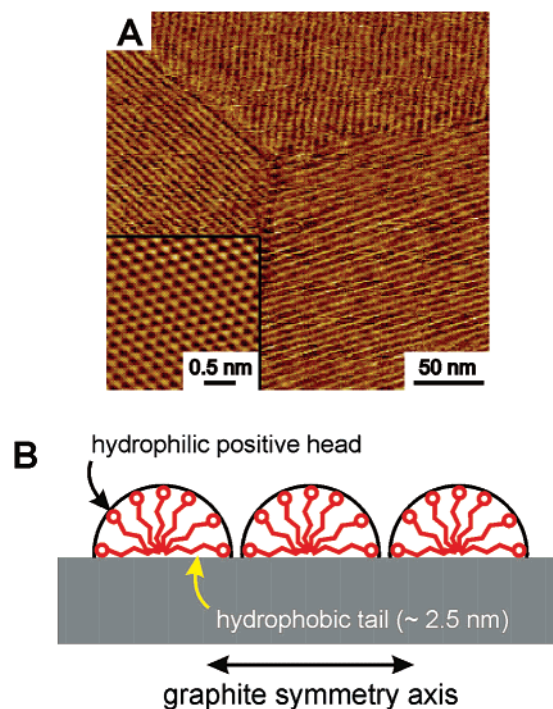‡ Department of Chemistry.

Figure 1. AFM image of hemi-cylindrical micellar assemblies of (A) cetyltrimethylammonium chloride (CTAC)[4] on HOPG. The underlying carbon lattice structure is shown in the inset in (A). The schematic side view (B) depicts hemi-cylindrical assemblies of CTAC. In the organized domains, the hemi-cylindrical rodlike micelles are aligned perpendicular to the symmetry axes.

templates.[16] Epitaxy,[17] quasi-epitaxy,[12] and van der Waals epitaxy[18] have been used to describe such ordered structures. Forrest[13] reviewed the potential energy (PE) calculation basis of orientational order for organic thin films where the adlayer energies of adjacent molecular units were lumped into simpler entities interacting with the substrate. However, simple addition of the PEs from isolated individual molecules on the crystalline surface is inadequate when dealing with crystal−water inter-
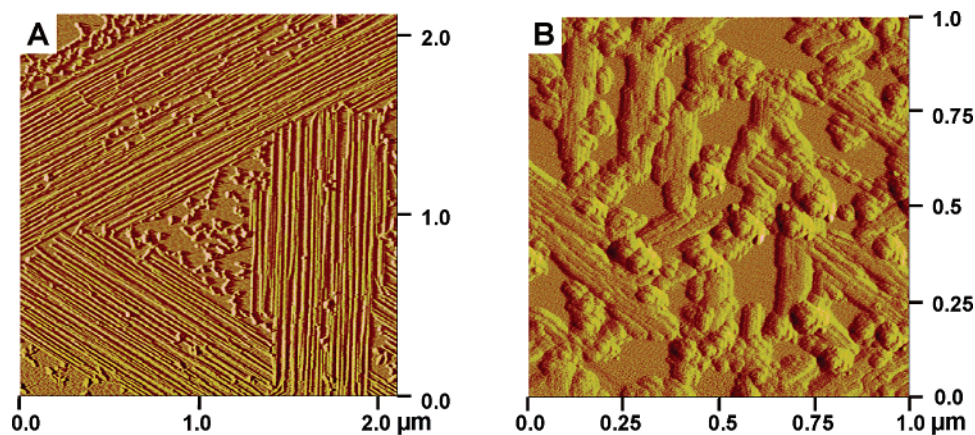
Figure 2. AFM images of a de novo designed β-sheet protein fibrils on HOPG (A) and amorphous carbon (B).[8] Each fibril is a linear array of 3.5-nm wide × 0.35-nm thick "strands".[10] The images show three distinct domains in (A) with orientations consistent with the symmetry axes of HOPG. It is noted that there are misalignments for short protein fibrils. Random orientations occur on amorphous carbon (B). In the de novo protein molecule, polar residues project up, and nonpolar residues project down. Note that dimensions in AFM images must be interpreted carefully to allow for effects of tip curvature.[9] (Reprinted with permission from ref 8. Copyright 2002 American Chemical Society).
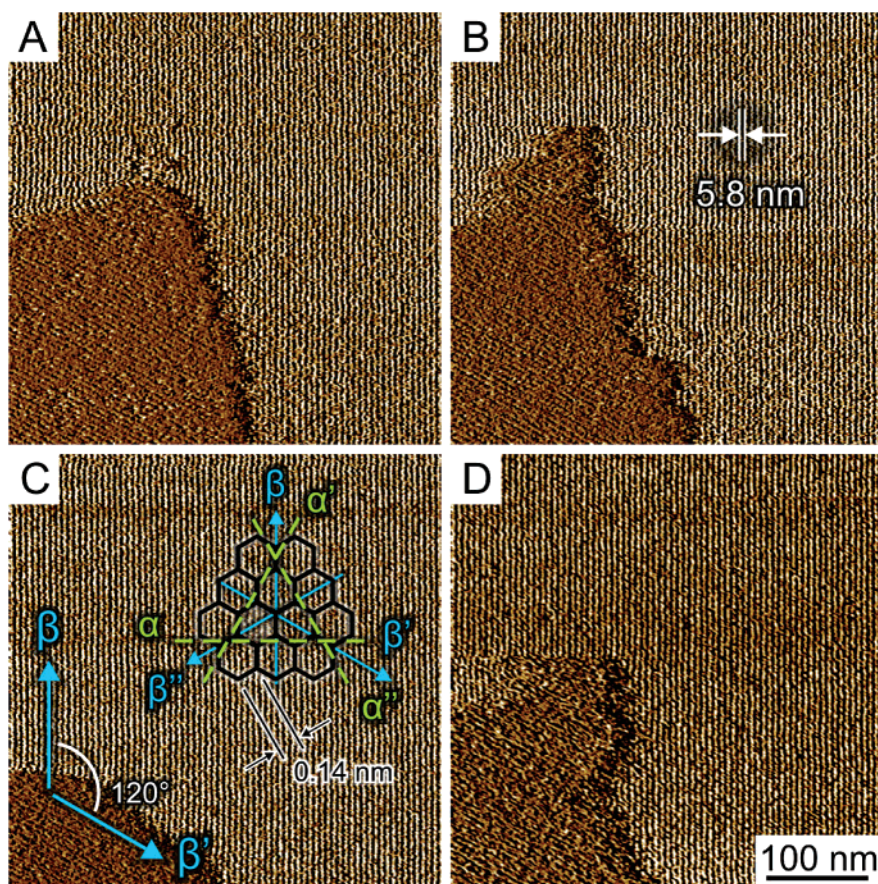

Figure 3. 500 nm × 500 nm AFM images of hemi-cylindrical surfactant aggregates formed on HOPG in a 10 mM CTAC solution.[7] Images A−D show the same area at intervals of 70 s. Note the dynamic competition between grains of two different angular orientations, β and β'. Panel C also depicts the three α and the three β directions (parallel and perpendicular to the symmetry axes of graphite) that define the underlying graphite lattice structure. After reaching thermal equilibrium the drift is less than 1 nm per min, and time-lapse imaging of a given region is possible. The AFM is a Multimode/Nanoscope IIIa, Veeco Instruments, Santa Barbara, CA. (Reprinted with permission from ref 7. Copyright 2006 American Physical Society).

faces, and thermal motion of the adsorbate plays an important role on its configuration at nonzero temperatures. Further, the pairwise summation of PE can be computationally intensive when applied to molecular assemblies (∼100 nm long or larger). The geometric lattice misfit schemes[14,15] developed as an alternate approach deal with sufficiently large molecular overlayers but do not give energy scales for different orientations. Thus, due to the lack of energetic considerations, these schemes predict orientations that are independent of the size of molecular assembly and cannot explain the misalignment for shorter protein fibrils shown in the interior region of Figure 2A. Moreover, the role of water and the fact that molecules access a large number of configurations at nonzero temperatures are not taken into account by these methods.

In a recent study,[7] we showed that the orientational order of CTAC hemi-cylindrical micelles at the graphite/water interface

is well defined although the micelles and surfactants are in continuous motion (Figure 3). Interaction energy calculations at the molecular level using pairwise summation showed that the orientational energy differences of a single surfactant are too small to explain anisotropic adsorption. In addition, Wanless and Ducker[19] demonstrated that the spacing of micelles on HOPG is not an integer multiple of the substrate unit cell which precludes a templation mechanism at molecular length scale as the governing mechanism. However, molecular assemblies show anisotropic organization despite the absence of a molecular-scale physical reason, suggesting that a more convincing explanation exists at micellar level. At the micellar (colloidal) level, a van der Waals torque on the micelles results from collective effects. The misalignment of shorter protein fibrils (Figure 2) also indicates that the anisotropic adsorption arises mainly from the energy difference for the larger assembly instead of an individual molecule. The dynamic character of molecular assembly during adsorption may be analogous to the continuous exchange of surfactants between micelles and bulk solution at small time scales.[20]

The goal of this paper is to expand on our earlier work so as to present a generalized theory for anisotropic adsorption of molecular assemblies at the colloidal length scale, including cylindrical and hemi-cylindrical geometries. The theory is based on the orientation of already extant rodlike molecular assemblies on the surface, corresponding to surfactant systems above the critical micelle concentration (CMC). In some cases, e.g., the work of Manne and Gaub,[3] spherical surfactant micelles exist in solution, whereas hemi-cylindrical micelles form on the surface. Although it is not clearly known how the assemblies form, evidently they arise from the locally high concentration of surfactants on and near the surface. Here, we treat orientation of preexisting rodlike micelles. On the colloidal length scale, we view the process as one where an entire assembly undergoes adsorption followed by rotation to a preferred orientation. The van der Waals interaction is implemented because it provides a credible mechanism for orientation with crystalline surfaces such as graphite.[21] We employ expressions for the van der Waals interaction between a macroscopic *rod* (i.e., the molecular assembly) parallel to the surface of an underlying (anisotropic) substrate. The overall interaction depends on the orientation of the rod with respect to the symmetry axes of the substrate and the separation between the (semi-infinite) substrate and the rod.

First, we develop a statistical model based on the balance between van der Waals and Brownian torques for calculation of the probability of a particular orientation. The model is then applied to two different molecular assemblies: hemi-cylindrical micelles and cylindrical protein fibrils. The calculations confirm that the torque experienced by a molecular aggregate is sufficient to overcome the Brownian forces so that an assembly aligns with respect to a symmetry axis of the graphite. Detailed treatments of the methodologies are given in the appendixes. Finally, we discuss the characteristics of molecular assembly such as its dynamic character, waviness, and interactions between assemblies. The formulation of the van der Waals interaction between a rod and an anisotropic surface is set out in the appendixes for cylindrical and hemi-cylindrical rods following the treatment by Parsegian and Weiss.[22] The detailed calculation of the dielectric properties of the graphite is also set out there, along with a discussion of the dielectric functions employed for the micelles and the protein fibrils.

A Probabilistic Description of Orientational Ordering. Anisotropic interactions between a cylindrical or hemi-cylindrical rod and a surface mimic those between a molecular assembly
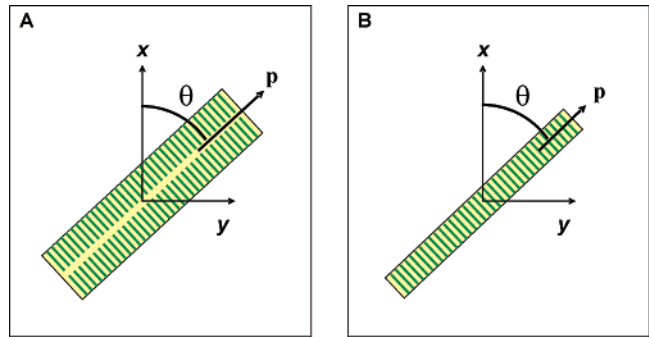

Figure 4. Schematic diagrams (top views) of orientations of: (A) a rodlike micelle and (B) a protein fibril as deduced from experimental observations.[2−9] The short lines inside the rectangles denote individual surfactant molecules in (A), and protein "strands" in (B). The micelle is a hemi-cylinder whose radius is the length of a surfactant molecule, while the fibril is approximated as a cylinder with a radius equal to half the length of a strand. Here *x* and *y* denote the directions parallel and perpendicular to one of the symmetry axes of the surface. The orientation of the rod is given by the director, **p**, lying parallel to the long axis of the assembly.

and an inorganic surface. The orientational ordering is pictured as follows. In solution, each molecule or assembly undergoes Brownian motion while being attracted to the surface by ubiquitous van der Waals forces. On the surface, rodlike structures form where the van der Waals interaction is anisotropic and induces a torque that alters the probability of a particular orientation. Near a surface, certain orientations are favored, and random rotational motion is suppressed. However, rotary motion parallel to the surface continues, and raft-like aggregates (cf. Figure 4) experience a van der Waals torque until they are aligned in an energy minimum.

To describe the rotational motion parallel to the surface, we use a Smoluchowski equation[23] to describe the evolution of the orientation probability distribution function, ψ, in a quiescent system, viz.,

$$\frac{\partial \psi}{\partial t} = D_r\left(\mathbf{p} \times \frac{\partial}{\partial \mathbf{p}}\right)\cdot\left[\mathbf{p} \times \frac{\partial \psi}{\partial \mathbf{p}} + \frac{\psi}{kT}\mathbf{p} \times \frac{\partial U}{\partial \mathbf{p}}\right] \quad (1)$$

Here the interaction energy, U, derives from van der Waals interactions, D_r represents the rotary diffusivity of a rodlike assembly, and **p** is a unit vector denoting the orientation. At equilibrium,

$$\frac{\partial \ln \psi}{\partial \mathbf{p}} = -\frac{1}{kT}\frac{\partial U}{\partial \mathbf{p}} \quad (2)$$

Accordingly, the balance between the torque associated with Brownian motion and the van der Waals interaction establishes the orientation probability distribution of the assembly.

As described in the appendixes, the van der Waals interaction energy between a cylindrical or hemi-cylindrical rod of length, l, and radius, a, and an anisotropic substrate is

$$U(R,\theta) = -\frac{A_H^{aniso}(\theta)a^2 l}{6R^3} \quad (3)$$

where $A_H^{aniso}(\theta)$ denotes a Hamaker constant with θ being the angle between the long axis of the rod and one of the symmetry axes of a substrate, as indicated in Figure 4. R denotes the separation between a cylindrical rod and a substrate or the separation between a hemi-cylindrical rod and surface. Here a and l denote the radius and length of the assembly. For rotational motion in the *xy* plane, it suffices to consider one component

of eq 2 and the probability distribution function can be found from solutions of

$$\frac{\partial \ln \psi}{\partial p_x} = -A' \frac{a^2 l}{6R^3} p_x \tag{4}$$

where A' is obtained from differentiation of the anisotropic Hamaker constant with respect to p_x, and scaled on kT. The right-hand side of eq 4 is proportional to the torque experienced by a rod at a certain separation R from the surface. From eq 4, the probability function ψ follows as

$$\psi = \tilde{C} \exp\left(-\frac{A'}{2} \frac{a^2 l}{6R^3} p_x^2\right) \tag{5}$$

where $\tilde{C}$ is an integration constant. Upon normalization, the probability density function $f(p_x)$ is

$$f(p_x) = \frac{\exp\left(-\frac{\hat{A}}{2} p_x^2\right)}{\int_0^1 \mathrm{d}\tilde{p}_x \exp\left(-\frac{\hat{A}}{2} \tilde{p}_x^2\right)} \tag{6}$$

with $\hat{A} = A' a^2 l/6R^3$. Clearly the probability density becomes uniform, i.e., $f(p_x) = 1$, for isotropic substrates where $\hat{A} = 0$. For $\hat{A} > 0$, the probability is maximum for $p_x = 0$ (where rods are aligned perpendicular to the symmetry axis) and a minimum at $p_x = 1$. Using the maximum and minimum probabilities, the tendency for the alignment of molecular assembly can be evaluated as the relative probability ratio:

$$\tilde{\gamma} = \frac{P_{\text{perpendicular}}}{P_{\text{parallel}}} = \exp\left(\frac{\hat{A}}{2}\right) \tag{7}$$

where P_{parallel} and $P_{\text{perpendicular}}$ denote probabilities for parallel and perpendicular configurations of the rod, respectively.

Anisotropic Adsorption of Micelles and Protein Fibrils. Next we look at two applications of the theory, first for micelles and then for protein fibrils. For hemi-cylindrical micelles on HOPG in an aqueous solution, we use the formulation for a hemi-cylindrical rod, eq A.24. The series representation for the Hamaker function A_H^{aniso} given in the appendix was summed into ultraviolet region ($\sim 10^{17}$ rad/s); the wave vector integration employed a 16-point Gauss−Laguerre quadrature method.[24] The data summarized in the appendix enable calculation of the dimensionless torque parameter A' for a hemi-cylindrical rod interacting with graphite across a thin film of water. When the rod is long and close to the surface, the relevant quantity $\hat{A}$ can be sizable even though A' is small, e.g., 1.991×10^{-5}.[7] Figure 5 depicts the relative probability as a function of the separation and assembly size. As expected, the relative probability ratio, i.e., the tendency for the alignment perpendicular to the symmetry axis of graphite, increases substantially as the separation decreases. In addition, since the hydrophobic side of the assembly faces the graphite, close separations are possible, and the probability may be even higher than those shown in Figure 5.

To analyze the orientation of protein fibrils, we use the formulation for a cylindrical rod, eq A.18 with the Hamaker function summed as before. Taking the radius of a fibril as half of the length of an individual protein strand (i.e., $a = 1.75$ nm) and $A' = 9.4614 \times 10^{-5}$, we calculate the relative probability ratio between the graphite surface and protein fibril for different fibril lengths and separations. Figure 6 shows the results for
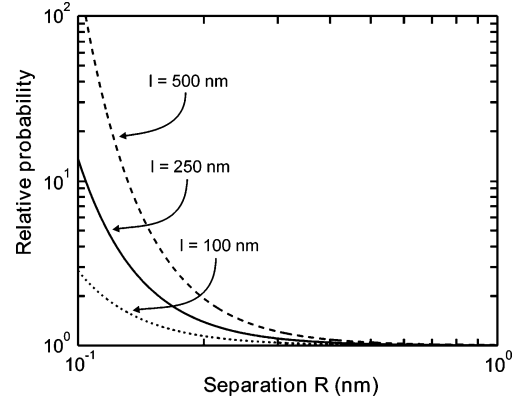

Figure 5. Relative probability relation for hemi-cylindrical micelles ($a = 2.5$ nm) of different lengths adsorbed on graphite as a function of separation between a hemi-cylindrical micelle and the surface. A large relative probability represents a strong tendency for alignment perpendicular to the symmetry axis of the graphite.
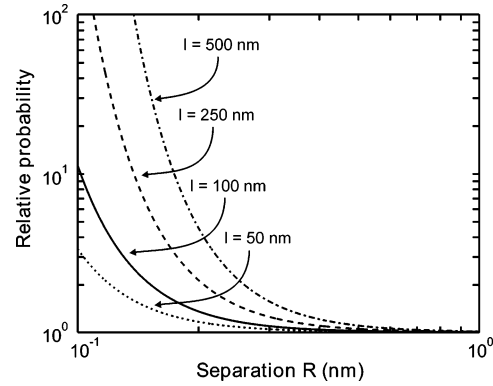

Figure 6. Relative probability relation for cylindrical rods ($a = 1.75$ nm) adsorbed on HOPG as a function of separation between a cylindrical rod and surface. A large relative probability represents a strong tendency for alignment of protein fibrils perpendicular to the symmetry axes of the graphite surface. Relative probabilities are larger than those for hemi-cylindrical cases due to the larger torque parameter arising from the greater mass associated with a full cylinder.
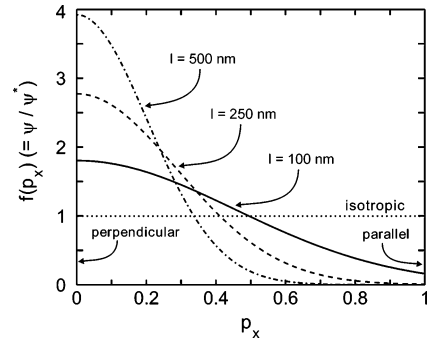

Figure 7. Probability density functions for cylindrical fibrillar structures of different lengths with a 0.1-nm separation from the surface. Note that $p_x = 0$ and 1 denote perpendicular and parallel alignments of the fibrillar structures with respect to the symmetry axis of the substrate.

four different lengths at different separations. Note that the relative probability increases significantly as the separation decreases.

Additional evidence for anisotropic adsorption is furnished by calculating the probability as a function of orientation at a particular separation. Figure 7 shows the results for three different fibril lengths. Interestingly, the relative probability for $l = 50$ nm (corresponding to 23 protein molecules stacked side by side) shown in Figure 6 is low even at very small separations,

$R \approx 0.1$ nm, suggesting that short assemblies should be disordered. This is consistent with the relatively misaligned 50−80 nm structures shown in the interior region of Figure 2A. The existence of the "critical" length suggests that a fibril should contain $O(100)$ molecules to experience an appreciable torque.

Taken together, these results suggest that the anisotropic adsorption of rodlike entities depicted in Figures 1−3 can be explained in terms of an anisotropic van der Waals interaction with the substrate.

Discussion

The theory presented in the previous sections improves our understanding of the anisotropic adsorption for both micelles and protein fibrils but does not cover some characteristics of molecular assembly: (i) the dynamic nature, (ii) micelle flexibility or waviness, and (iii) interactions between assemblies. In this section, we discuss each and its implication for the theory.

Dynamic Character of Molecular Assembly. In the present theory, we neglect the dynamics of the micelle disintegration and reassembly shown in Figure 3 and discussed in our previous paper.[7] The dynamic behavior of the micelle results from molecular motions such as continuous exchange of surfactants between micelles on the surface and in the bulk solution. The exchange would be more significant at grain boundaries because two different micellar orientations at the boundary give rise to the discontinuity of micelles that was known to be energetically unstable.[1] The time scale for the dynamics of surfactant molecule is typically $O(10^{-6})$ s,[25] while the time scale associated with the orientation is $O(10^{-4})$ s (from the inverse of the rotary diffusivity for 100 nm of molecular assembly).[23] Consequently, the micelles are indeed in quasi-equilibrium at the rotational time scale, which allows us to investigate the process by considering a micelle as the moiety of interest.

However, to gain a complete understanding of the anisotropic adsorption, we should employ a temporal change of length of the molecular assembly due to continuous disintegration and reformation of molecular assembly. The temporal change of length might be treated as a "reaction" of molecular assembly whose rate constant is related to the disintegration and reformation energies of the molecular assembly.[26] Combined with eq 1, we would obtain a temporal orientational probability distribution as a function of time and length of molecular assembly as well as other parameters. The temporal change of the length affects the tendency for the alignment over time, and understanding of these processes would help resolve the dynamic behavior of the anisotropic adsorption.

Flexibility or Waviness of Molecular Assembly. The theory presented above describes molecular assemblies as rigid rods. Molecular assemblies are, however, inherently "flexible" or "wavy" owing to an existence of a finite persistence length. A persistence length of rodlike molecular assembly can be understood as a length scale where elastic and thermal energies are in balance. The persistence length is typically $O(10)$ nm for cylindrical micelle[27] and $O(100)$ nm for the protein fibril[10] in aqueous solutions. Taking account of the waviness into the theory, we view a wavy molecular assembly as connected rods whose lengths are comparable to the persistence length near surface. In this description, while the "overall" rotational motion of whole molecular assembly is determined by the "overall" van der Waals torque, a van der Waals torque on each segment, collectively, straightens the whole molecular assembly. Here the overall rotational motion can be defined by the end-to-end director of the assembly. Since the energy associated with the waviness can be represented by a bending energy of molecular

assembly,[28] a balance between the bending energy and the van der Waals torque determines the straightness of the whole molecular assembly. When a van der Waals torque on each segment is not sufficient to overcome the bending energy of molecular assembly, a wavy orientational ordering of molecular assembly would occur, which may qualitatively explain the meandering of the anisotropic adsorption of CTAC micelle on mica surface.[4]

Interaction between Molecular Assemblies. Although the theory is focused, for simplicity, on the orientational behavior of an isolated molecular assembly, experimental observations (Figures 1−3) show large patches with the same directionality. The three symmetry axes of the substrate are dielectrically equivalent so that a symmetry-breaking term is needed to form the unidirectional large patch. For an isolated molecular assembly, the only interaction comes from the surface. However, when the assemblies exist on the surface, the configuration of an assembly is determined not only by the interaction with the surface but also by interactions between assemblies. The minimum energy configuration between rodlike molecular assemblies occurs when they are in parallel,[29] and thus the large unidirectional patch can be formed. As a first approximation, the effect of interaction between molecular assemblies on the orientational order might be examined by superimposing an additional energy term in U in eq 1. Note that the interaction between molecular assemblies can be implemented along with the temporal change of the length, although the interaction between molecular assemblies is described on "quasi-equilibrium".

Conclusions

We have set out a detailed theory for the anisotropic adsorption of molecular assemblies on crystalline surfaces. A particular orientation is favored because rotational motion is influenced by a van der Waals torque; orientation arises from the interaction between an anisotropic object (a rod) and an anisotropic substrate. Although the intrinsic torque parameter is small, the combination of a relatively large rod volume and close separation provides the necessary torque. The theory presented provides an explicit relationship between the energy and the orientational order, involving simple geometry and physical properties. The theory also captures the essential features of the anisotropic adsorption of a molecular assembly and provides a basic formalism to which further detailed considerations can be incorporated, such as the dynamic character of molecular assemblies, the waviness of molecular assemblies, the interaction between molecular assemblies.

Appendices

A. Formulation of the van der Waals Interaction between a Rod and an Anisotropic Surface. To mimic interactions between a rod and an inorganic surface we employ the notion of an anisotropic dielectric permeability. First, in section A.1, we calculate the van der Waals interaction between two semi-infinite slabs in an isotropic medium using the Lifshitz methodology set out by Parsegian and Weiss.[22] One body is a
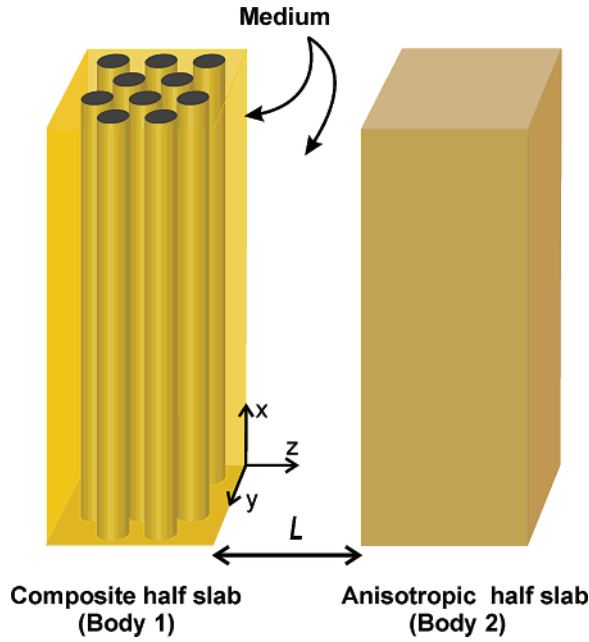
Figure A.1. A schematic diagram showing two semi-infinite slabs embedded in an isotropic medium. Body-1 consists of isotropic rods (radius a) in an isotropic medium; body-2 is an anisotropic slab. The distance between the slabs is L.

composite consisting of an *array* of dielectrically isotropic rods embedded in an identical medium; the other is a semi-infinite slab with an intrinsic dielectric anisotropy. Next, in section A.2, we derive an expression for the anisotropic van der Waals interaction between an individual rod and a semi-infinite slab. The anisotropic interaction between a hemi-cylindrical rod and a surface is set out in section A.3.

A.1. The van der Waals Interaction between Semi-Infinite, Anisotropic Slabs. Consider the two semi-infinite slabs depicted in Figure A.1. Body-1 is a composite semi-infinite slab composed of rods embedded in an isotropic medium; body-2 is an intrinsically anisotropic semi-infinite slab. The intervening aqueous medium is isotropic, and its dielectric tensor $\mathbf{P}^m$ is $\epsilon_m \mathbf{I}$ where $\mathbf{I}$ is the unit tensor. Each rod is isotropic, and its dielectric tensor can be expressed as $\mathbf{P}^r = \epsilon_r \mathbf{I}$. Thus, for the composite semi-infinite slab, the dielectric tensor $\mathbf{P}^1$ is:

$$\begin{pmatrix} A & 0 & 0 \\ 0 & B & 0 \\ 0 & 0 & B \end{pmatrix}$$

where the components parallel and perpendicular to the rods (A and B) can be represented as $\epsilon_m + v(\epsilon_r - \epsilon_m)$ and $\epsilon_m + 2v\epsilon_m\Delta_{rm}/(1 - v\Delta_{rm})$, respectively.[29] Here Δ_{rm} denotes $(\epsilon_r - \epsilon_m)/(\epsilon_r + \epsilon_m)$, and v is the fractional density of rods, $N\pi a^2$, where N is the number of rods per unit cross-section. Note that $v \ll 1$. Furthermore, the composite semi-infinite slab is anisotropic (with uniaxial symmetry) due to the geometric anisotropy of the rods.

For the anisotropic slab, the dielectric tensor $\mathbf{P}^2$ is:

$$\begin{pmatrix} \alpha & 0 & 0 \\ 0 & \beta & 0 \\ 0 & 0 & \gamma \end{pmatrix}$$

The other important assumption is that the dielectric axes of two bodies perpendicular to the surfaces of the slabs coincide with each other. This allows us to characterize the dielectric

tensor of body 2 by an angle θ.[22] In other words, the angle θ can be considered as the mutual angle between the directions of A and α.

Now that we have two anisotropic semi-infinite slabs, we can take advantage of results by Parsegian and Weiss,[22] obtained from solving the Maxwell equations. Accordingly, the interaction between such slabs in an isotropic media can be represented as:

$$E(L,\theta) =$$

$$\frac{kT}{16\pi^2 L^2}{\sum_{n=0}^{\infty}}' \int_0^{2\pi} d\phi \int_0^{\infty} \ln[1 - \Delta_n^2(\theta,\phi)e^{-x}]x \, dx \quad \text{(A.1)}$$

where $E(L,\theta)$ denotes the interaction between two slabs, L is the separation distance, k is Boltzmann's constant, and T is the temperature. The sum is over all n electromagnetic field modes (i.e., frequency modes) that satisfy the boundary conditions; ϕ is an angle of a wave vector in polar coordinate system. The integration variable is $x \equiv 2qL$, where q denotes the magnitude of the wave vector. The prime in the summation indicates that the $n = 0$ term is to be multiplied by 1/2. Here $\Delta_n^2(\theta,\phi)$ can be represented as:

$$\Delta_n^2(\theta,\phi) = \left(\frac{\tilde{a} - 1}{\tilde{a} + 1}\right)\left(\frac{\tilde{b} - 1}{\tilde{b} + 1}\right) \quad \text{(A.2)}$$

where

$$\tilde{a} = \frac{B}{\epsilon_m}\sqrt{1 + \frac{(A - B)}{B}\cos^2\phi} \quad \text{(A.3)}$$

and

$$\tilde{b} = \frac{\gamma}{\epsilon_m}\sqrt{\frac{\beta}{\gamma} + \frac{(\alpha - \beta)}{\gamma}\cos^2(\theta - \phi)} \quad \text{(A.4)}$$

Next, substituting $\tilde{a}$ and $\tilde{b}$ into eq A.2 and introducing $\delta_3 \equiv (A - B)/B$, $\kappa \equiv (\alpha - \beta)/\beta$ and $\delta_1 \equiv \beta/\gamma$, enables $\Delta_n^2(\theta,\phi)$ to be rewritten as:

$$\Delta_n^2(\theta,\phi) = \left(\frac{\epsilon_m - B\sqrt{1 + \delta_3\cos^2\phi}}{\epsilon_m + B\sqrt{1 + \delta_3\cos^2\phi}}\right)$$
$$\left(\frac{\epsilon_m - \gamma\delta_1^{1/2}\sqrt{1 + \kappa\cos^2(\theta - \phi)}}{\epsilon_m + \gamma\delta_1^{1/2}\sqrt{1 + \kappa\cos^2(\theta - \phi)}}\right) \quad \text{(A.5)}$$

Given a small difference between α and β, κ and δ_3 can be expanded in terms of v as

$$\delta_3 \sim v\left[\frac{\epsilon_r - \epsilon_m}{\epsilon_m} - 2\Delta_{rm}\right] + O(v^2) \quad \text{(A.6)}$$

Expanding eq A.5 in terms of κ and δ_3 provides a simplified relation for $\Delta_n^2(\theta,\phi)$:

$$\Delta_n^2(\theta,\phi) = PR + \delta_3 QR\cos^2\phi + \kappa PS\cos^2(\theta - \phi) +$$
$$\kappa\delta_3 QS\cos^2\phi\cos^2(\theta - \phi) \quad \text{(A.7)}$$

P, Q, R, and S depend on the dielectric properties of a rod, medium, and anisotropic semi-infinite slab as follows:

$$P = \frac{\epsilon_m - B}{\epsilon_m + B} \tag{A.8}$$

$$Q = \left(\frac{B^2 - B\epsilon_m}{\epsilon_m^2 - B^2} + \frac{B^2}{(\epsilon_m + B)^2} \right) \tag{A.9}$$

$$R = \frac{\epsilon_m - \gamma\delta_1^{1/2}}{\epsilon_m + \gamma\delta_1^{1/2}} \tag{A.10}$$

$$S = \left(\frac{\gamma - \epsilon_m\delta_1^{1/2}}{\epsilon_m^2 - \gamma^2\delta_1} + \frac{\gamma}{(\epsilon_m + \gamma\delta_1^{1/2})^2} \right)\gamma\delta_1 \tag{A.11}$$

Equation A.1 can be simplified by taking dominant term in the series, viz., $\ln[1 - \Delta_n^2(\theta,\phi)\, e^{-x}] \sim - \Delta_n^2(\theta,\phi)\, e^{-x}$. After integrating with respect to ϕ, the interaction between two anisotropic semi-infinite slabs in an isotropic medium is:

$$E(L,\theta) = -\frac{kT}{16\pi L^2}\sum_{n=0}^{\infty}{}'$$
$$\int_0^{\infty} \left(2PR + \kappa PS + \delta_3 QR + \frac{(1 + 2\cos^2\theta)}{4}\kappa\delta_3 QS \right) x\, e^{-x}\, dx \tag{A.12}$$

It is noteworthy that the interaction shows an explicit angular dependence due to the anisotropic nature of two slabs. On the other hand, when we have an isotropic spherical particle, the angular dependence vanishes because $A = B$ or equivalently, $\delta_3 = 0$. Accordingly, the geometrical anisotropy of the particle and dielectric anisotropy of the surface are crucial ingredients in the angular dependence shown in eq A.12.

A.2. The van der Waals Interaction between a Rod and Anisotropic Semi-Infinite Slab. The next step is to obtain the interaction between a single rod and the anisotropic semi-infinite slab from $E(L,\theta)$. Since the volume fraction of the rods in body 1 (the composite semi-infinite slab) is very small, we can relate $V(R,\theta)$ with $E(L,\theta)$ a pairwise summation analogous to Hamaker's calculation:

$$E(L,\theta) = N\int_{-\infty}^{0} dz\, V(R,\theta) \tag{A.13}$$

Here z is measured perpendicular to the surfaces of the composite and anisotropic semi-infinite slab; $z = 0$ and $z = L$ correspond to the surfaces of the composite and anisotropic semi-infinite slabs, respectively; the separation between a cylindrical rod and surface, $R = z + L$. Thus, the interaction follows from $V(R,\theta)$ via a pairwise summation between a rod and the anisotropic semi-infinite slab. Then, from eq A.13, we obtain $V(R,\theta)$ as

$$V(R,\theta) = -\frac{1}{N}\left(\frac{\partial E(L,\theta)}{\partial L} \right)_{L=R} \tag{A.14}$$

Before we calculate $V(R,\theta)$, we can show the explicit $O(v)$-dependence of each term in eq A.12. Consider P, Q, R, and S in eq A.12. Obviously, R and S are $O(1)$ to leading order because they are related to the dielectric character of the anisotropic semi-infinite slab (body 2). Expansions of P and Q in terms of v give:

$$P \approx -v\Delta_{rm} + O(v^2) \tag{A.15}$$

and

$$Q \approx -\frac{1}{4} + O(v) \tag{A.16}$$

Since P is $O(v)$ and Q is $O(1)$, all the terms in the summation bracket in eq A.12 are $O(v)$, which implies that the pairwise summation is appropriate. Using eq A.13 and leading order expressions for P, Q, R, and S, we obtain the interaction between a single rod and an anisotropic semi-infinite slab $V(R,\theta)$ in terms of the dielectric properties of a rod, medium, and anisotropic semi-infinite slab:

$$V(R,\theta) =$$
$$-\frac{kTa^2 l}{8R^3}\sum_{n=0}^{\infty}{}'\int_0^{\infty} dx\, x\, e^{-x}\left[2\left(\frac{\epsilon_m - (\beta\gamma)^{1/2}}{\epsilon_m + (\beta\gamma)^{1/2}} \right)\left(\frac{\epsilon_m - \epsilon_r}{\epsilon_m + \epsilon_r} \right) + \right.$$
$$\frac{1}{4}\left(\frac{\epsilon_m - (\beta\gamma)^{1/2}}{\epsilon_m + (\beta\gamma)^{1/2}} \right)(\epsilon_m - \epsilon_r)\left(\frac{1}{\epsilon_m} - \frac{2}{\epsilon_m + \epsilon_r} \right) +$$
$$\left(\frac{\gamma - \epsilon_m(\gamma/\beta)^{1/2}}{\epsilon_m^2 - \beta\gamma} + \frac{\gamma}{(\epsilon_m + (\beta\gamma)^{1/2})^2} \right)(\alpha - \beta)\left(\frac{\epsilon_m - \epsilon_r}{\epsilon_m + \epsilon_r} \right) +$$
$$\frac{(1 + 2\cos^2\theta)}{16}\left(\frac{\gamma - \epsilon_m(\gamma/\beta)^{1/2}}{\epsilon_m^2 - \beta\gamma} + \frac{\gamma}{(\epsilon_m + (\beta\gamma)^{1/2})^2} \right) \times$$
$$\left. (\alpha - \beta)(\epsilon_m - \epsilon_r)\left(\frac{1}{\epsilon_m} - \frac{2}{\epsilon_m + \epsilon_r} \right) \right] \tag{A.17}$$

where l is the length of a rod. After rearranging and simplifying eq A.17, the anisotropic Hamaker constant A_H^{aniso} follows as

$$A_H^{aniso} = \frac{3}{4}kT\sum_{n=0}^{\infty}{}'\int_0^{\infty} dx\, xe^{-x}\left(\frac{\epsilon_m - \epsilon_r}{\epsilon_m + \epsilon_r} \right)\frac{1}{(\epsilon_m + (\beta\gamma)^{1/2})^2}$$
$$\left[\frac{(7\epsilon_m + \epsilon_r)(\epsilon_m^2 - \beta\gamma)}{4\epsilon_m} - (\beta\gamma)^{1/2}\epsilon_m\left(\frac{\alpha - \beta}{\beta} \right) + \right.$$
$$\left. \frac{(1 + 2\cos^2\theta)}{16}\left(\frac{\alpha - \beta}{\beta} \right)(\epsilon_m - \epsilon_r)(\beta\gamma)^{1/2} \right] \tag{A.18}$$

Thus, the interaction energy can be rewritten in terms of the anisotropic Hamaker constant as

$$V(R,\theta) = -\frac{A_H^{aniso} a^2 l}{6R^3} \tag{A.19}$$

Note that R denotes the separation between a cylindrical rod and surface. For an isotropic semi-infinite slab (body-2), eq A.18 reduces to

$$A_H^{aniso} = \frac{3}{2}kT\sum_{n=0}^{\infty}{}'\int_0^{\infty} dx\, x\, e^{-x}\left(\frac{\epsilon_m - \epsilon_r}{\epsilon_m + \epsilon_r} \right)\left(\frac{\epsilon_m - (\beta\gamma)^{1/2}}{\epsilon_m + (\beta\gamma)^{1/2}} \right) \tag{A.20}$$

Since the anisotropic dielectric property stems from the spatial dispersion (i.e., the wave vector dependence) of the crystalline substrate, it can be calculated from methods outlined in appendix B. The angular dependence in eq A.18 is determined by summations over both the wave vectors and frequencies.

A.3. The van der Waals Interaction between a Hemi-Cylindrical Rod and Anisotropic Surface. Assuming that the planar side of a hemi-cylinder faces the surface, one can approximate an anisotropic van der Waals interaction for a hemi-cylindrical rod, similar to that for a cylindrical rod as described in section A.2. One important difference between a hemi-cylinder and a cylinder is that the hemi-cylinder induces dielectric anisotropy in the y and z directions so that the three principal components of dielectric tensor for $\mathbf{P}^1$ of the composite slab (Figure A.1) are all different. Following the formulation used before, consider a cylindrical rod whose dielectric tensor is $\mathbf{P}^r = \epsilon_r \mathbf{I}$ in one-half of the cross section and $\mathbf{P}^m = \epsilon_m \mathbf{I}$ in the other. The dielectric tensor $\mathbf{P}^1$ in the directions of principal axes becomes:

$$\begin{pmatrix} A & 0 & 0 \\ 0 & B & 0 \\ 0 & 0 & C \end{pmatrix}$$

where the components parallel to the hemi-cylinders (A) and perpendicular to the hemi-cylinders (B and C) are dependent on the dielectric properties of the hemi-cylinder and the isotropic medium and volume fraction $v = N\pi a^2$ as

$$A = \epsilon_m + v\frac{(\epsilon_r - \epsilon_m)}{2} \tag{A.21}$$

$$B = \epsilon_m + 2\epsilon_m v\frac{(\epsilon_r - \epsilon_m)}{(\epsilon_r + 3\epsilon_m)} \tag{A.22}$$

$$C = \epsilon_m + 2\epsilon_m v\frac{(\epsilon_r - \epsilon_m)}{(3\epsilon_r + \epsilon_m)} \tag{A.23}$$

Following the development set out in sections A.1 and A.2, we obtain the anisotropic Hamaker constant and van der Waals interaction as

$$A_H^{aniso} = \frac{3}{4}kT\sum_{n=0}^{\infty}{}' \int_0^{\infty} dx\, x\, e^{-x} \frac{(\epsilon_m - \epsilon_r)}{(\epsilon_m + (\beta\gamma)^{1/2})^2}$$
$$\left[\frac{(47\epsilon_m^2 + 14\epsilon_m\epsilon_r + 3\epsilon_r^2)(\epsilon_m^2 - \beta\gamma)}{8\epsilon_m(3\epsilon_r + \epsilon_m)(\epsilon_r + 3\epsilon_m)} - (\beta\gamma)^{1/2}\frac{\epsilon_m}{3\epsilon_r + \epsilon_m} \right.$$
$$\left. \left(\frac{\alpha - \beta}{\beta}\right) + \frac{(1 + 2\cos^2\theta)}{16}\left(\frac{\alpha - \beta}{\beta}\right)\frac{(\epsilon_m - \epsilon_r)}{2(\epsilon_r + 3\epsilon_m)}(\beta\gamma)^{1/2} \right] \tag{A.24}$$

and

$$V(R,\theta) = -\frac{A_H^{aniso} a^2 l}{6R^3} \tag{A.25}$$

Here R is the separation between the hemi-cylinder and surface, and a is the radius of the hemi-cylinder. The Hamaker constant shown in eq A.24 approximates the hemi-cylinder case because dielectric properties of the bottom half of the hemi-cylinder and the intervening medium are identical. The identical dielectric property gives rise to less interaction compared to that of the cylinder as well. Notice that the xy character in $\mathbf{P}^1$ (eqs A.21−A.23) induces an angular dependence on the anisotropic Hamaker constant (eq A.24). For an isotropic semi-infinite slab (body-2), eq A.24 becomes

$$A_H^{aniso} = \frac{3}{2}kT\sum_{n=0}^{\infty}{}' \int_0^{\infty} dx\, xe^{-x}\left(\frac{\epsilon_m - \epsilon_r}{\epsilon_m + 3\epsilon_r}\right)\left(\frac{\epsilon_m - (\beta\gamma)^{1/2}}{\epsilon_m + (\beta\gamma)^{1/2}}\right) \tag{A.26}$$

B. Dielectric Functions for Water, Protein, Surfactant, and Graphite. To calculate the Hamaker constant using the formulations set out in the A appendixes, one needs to know the dielectric response functions for the suspending medium (water), the rods (protein or surfactant), and the substrate (graphite). For water, the dielectric response function can be modeled by Debye rotational relaxation term and Lorentz harmonic-oscillator absorption terms up to ultraviolet frequency:[30]

$$\epsilon_{water}(i\xi_n) =$$
$$1 + \frac{d_0}{1 + \xi_n/\omega_0} + \sum_{j=1}^{11}\frac{f_j}{1 + g_j(\xi_n/\omega_j) + (\xi_n/\omega_j)^2} \tag{B.1}$$

where d_0 and f_j represent the oscillator strengths for the rotational relaxation and infrared and ultraviolet absorption, ω_0 and ω_j are resonance frequencies, and g_j is the bandwidth. Here $\xi_n = 2\pi kTn/\hbar$ where $\hbar$ is the Planck's constant divided by 2π, and n is a nonnegative integer. Numerical values of oscillator parameters are tabulated in the literature.[30] We assume a hydrocarbon-like dielectric response for proteins.[31] Hydrocarbons typically have one absorption peak in the ultraviolet so the dielectric response function of the protein or surfactant is:[32]

$$\epsilon_{protein\ or\ surfactant}(i\xi_n) = 1 + \frac{f}{1 + (\xi_n/\omega)^2} \tag{B.2}$$

where $f = 1.0$ and $\omega = 1.5 \times 10^{16}$ (rad/s).

Graphite requires a more elaborate consideration. Since the hexagonal lattice belongs to the class of uniaxial crystal structures, the optical properties of in-plane dielectric response are equal, i.e., $\alpha(\omega) = \beta(\omega)$. However, when the separation between two slabs is of an order of nanometers, electromagnetic modes of wavelength comparable to interatomic spacing become important, and it turns out that the full dielectric function, which has both frequency and wave vector dependence, has to be considered. The anisotropy of the in-plane dielectric function is generated via the wave vector $\mathbf{q}$, and therefore we shall denote the two components of the dielectric tensor by $\alpha(\omega,q_x)$ and $\beta(\omega,q_y)$. Perpendicular to the graphite layer (the extraordinary axis) the dielectric response function $\gamma(\omega,\mathbf{q})$ has weak dependence on wave vector so that the oscillator model[33] provides an adequate description, i.e., $\gamma(\omega,\mathbf{q}) \approx \gamma(\omega,\mathbf{q} = 0)$. Within the random-phase approximation, the dielectric response function for $\alpha(\omega,q_x)$ and $\beta(\omega,q_y)$ of a two-dimensional graphite layer is given by

$$\epsilon_{graphite}(\omega,\mathbf{q}) = 1 - \frac{4\pi e^2}{q}\sum_{n,n'}\int_{1st\ BZ}\frac{d^2k}{(2\pi)^2}|\langle n',\mathbf{k} +$$
$$\mathbf{q}|\ e^{i\mathbf{q}\cdot\mathbf{r}}|n,\mathbf{k}\rangle|^2\frac{f(E_{n',\mathbf{k}+\mathbf{q}}) - f(E_{n,\mathbf{k}})}{E_{n',\mathbf{k}+\mathbf{q}} - E_{n,\mathbf{k}} - (\omega + i\Gamma)} \tag{B.3}$$

where f is the Fermi distribution function and Γ represents broadening in the absorption spectrum. The matrix element $\langle n',\mathbf{k} + \mathbf{q}|\ e^{i\mathbf{q}\cdot\mathbf{r}}|n,\mathbf{k}\rangle$ represents an integral over $\mathbf{r}$, which is a position vector in real space. The summation denoted by n,n' is over all valence and conduction bands; the integration is over crystal momentum $\mathbf{k}$ in the first Brillouin zone. The calculation can be carried out either by the tight-binding model[34] or from first-

TABLE B.1: Comparison between the Current Methodology and Extant Results for Several Systems in Terms of A_H^{iso}

	current methodology[a]	experimental results	other theoretical calculations
graphite−water−graphite	24	12.1−24[37,38]	28[39]
graphite−air−graphite	53	51−143[40]	61[39]
hydrocarbon−water−hydrocarbon	1.0	~1.2[1]	−

[a] The frequency mode summation is carried up to the ultraviolet region ($\sim10^{17}$ (rad/s)) at 300 K. For graphite, β was obtained at the zero wave vector limit.

principles method.[35] We adopted the tight-binding model approach in the current study. The energy levels $E_{n,\mathbf{k}}$ and other tight-binding parameters can be taken from the first-principles calculation. For energies below 15 eV, Lin et al.[34] showed the anisotropic dielectric response function of graphite for several wave vectors. In general, the imaginary dielectric response functions, $\alpha(i\xi_n,q_x)$ and $\beta(i\xi_n,q_y)$, are monotonically decreasing functions in the imaginary frequency $i\xi_n$. Their magnitudes also become smaller as $\mathbf{q}$ grows larger, so we model the wave vector dependence of $\gamma(i\xi_n,\mathbf{q})$ similar to the trend in α and β.

As a check of the calculated dielectric response functions, we used eq A.20 to evaluate Hamaker constants for several systems. Further discussion of the dielectric function of graphite can be found in Li et al.[36] Results are shown in Table B.1; our calculations are in accord with the experimental and theoretical results.[1,37−40]

The polar groups of the protein or surfactant molecule, which originate an intrinsic permanent dipole moment, merit a further comment here. We can set $f = 1.0$ and $\omega = 1.5 \times 10^{16}$(rad/s) for a typical nonpolar hydrocarbon in eq B.2. However, in the examples of the de novo designed protein,[8] one side of the β-sheet is made up of polar and charged residues. In the presence of charged residues, there will be counterions to neutralize the protein. As a result, the protein has a permanent dipole moment, and interactions of Debye-type (dipole−induced dipole) should be considered as a driving force in the orientational ordering of the self-assembly structure. In such cases, the mobile counterions near charged amino acids will give rise to a random and fluctuating dipole moment. The polarizability, and hence the magnitude of the dielectric response function, would be larger than the values we employed here. For a proper choice of f and ω in eq B.2, the treatment in sections A and B can be carried over to a more general case where polar molecules are involved. In view of a larger dielectric constant, a larger anisotropy in the van der Waals interaction is expected.

References and Notes

(1) Israelachvili, J. *Intermolecular and Surface Forces*; Academic Press: Boston, 1992.

(2) Manne, S.; Cleveland, J. P.; Gaub, H. E.; Stucky, G. D.; Hansma, P. K. *Langmuir* **1994**, *10*, 4409.

(3) Manne, S.; Gaub, H. E. *Science* **1995**, *270*, 1480.

(4) Aksay, I. A.; Trau, M.; Manne, S.; Honma, I.; Yao, N.; Zhou, L.; Fenter, P.; Eisenberger, P. M.; Grunner, S. M. *Science* **1996**, *273*, 892.

(5) Wanless, E. J.; Ducker, W. A. *J. Phys. Chem.* **1996**, *100*, 3207.

(6) Patrick, H. N.; Warr, G. G.; Manne, S.; Aksay, I. A. *Langmuir* **1997**, *13*, 4349.

(7) Saville, D. A.; Chun, J.; Li, J.-L.; Schniepp, H. C.; Car, R.; Aksay, I. A. *Phys. Rev. Lett.* **2006**, *96*, 18301.

(8) Brown, C. L.; Aksay, I. A.; Saville, D. A.; Hecht, M. H. *J. Am. Chem. Soc.* **2002**, *124*, 6846.

(9) Brown, C. L. Bachelor of Arts Thesis; Princeton University, Princeton, New Jersey, 2001.

(10) West, M. W.; Wang, W.; Patterson, J.; Mancias, J. D.; Beasley, J. R.; Hecht, M. H. *Proc. Natl. Acad. Sci. U.S.A.* **1999**, *96*, 11211.

(11) Novaco, A. D.; McTague, J. P. *Phys. Rev. Lett.* **1977**, *38*, 1286.

(12) So, F. F.; Forrest, S. R. *Phys. Rev. Lett.* **1991**, *66*, 2649.

(13) Forrest, S. R. *Chem. Rev.* **1997**, *97*, 1793.

(14) Last, J. A.; Hooks, D. E.; Hillier, A. C.; Ward, M. D. *J. Phys. Chem. B* **1999**, *103*, 6723.

(15) Ward, M. D. *Chem. Rev.* **2001**, *101*, 1697.

(16) Rabe, J. P.; Buchholz, S. *Science* **1991**, *253*, 424.

(17) Hara, M.; Sasabe, H.; Yamada, A.; Garito, A. F. *Jpn. J. Appl. Phys.* **1989**, *28*, L309.

(18) Koma, A. *Surf. Sci.* **1992**, *267*, 29.

(19) Wanless, E. J.; Ducker, W. A. *Langmuir* **1997**, *13*, 1463.

(20) Evans, D. F.; Wennerström, H. *The Colloidal Domain*; VCH Publishers: New York, 1994.

(21) Interactions due to permanent dipoles may also play a role in anisotropic adsorption. The methodology set out here can be generalized to include such contributions, cf., Appendix B.

(22) Parsegian, V. A.; Weiss, G. H. *J. Adhesion* **1972**, *3*, 259.

(23) Doi, M.; Edwards, S. F. *The Theory of Polymer Dynamics*; Clarendon Press: Oxford, 1986.

(24) Press, W. H.; Teukolsky, S. A.; Vetterling, W. T.; Flannery, B. P. *Numerical Recipes in FORTRAN*; Cambridge University Press: Cambridge, 1992.

(25) Hunter, R. J. *Foundations of Colloid Science*; Clarendon Press: Oxford, 1986; Vol. I.

(26) Cates, M. E. *Macromolecules* **1987**, *20*, 2289.

(27) Cates, M. E.; Candau, S. J. *J. Phys.: Condens. Matter* **1990**, *2*, 6869.

(28) Landau, L. D.; Lifshitz, E. M. *Theory of Elasticity*; Pergamon Press: New York, 1986.

(29) Parsegian, V. A. *J. Chem. Phys.* **1972**, *56*, 4393.

(30) Russel, W. B.; Saville, D. A.; Schowalter, W. R. *Colloidal Dispersions*; Cambridge University Press: New York, 1989.

(31) Honig, B.; Nicholls, A. *Science* **1995**, *268*, 1144.

(32) Mahanty, J.; Ninham, B. W. *Dispersion Forces*; Academic Press: New York, 1976.

(33) Djurisic, A. B.; Li, E. H. *J. Appl. Phys.* **1999**, *85*, 7404.

(34) Lin, M. F.; Huang, C. S.; Chou, D. S. *Phys. Rev. B* **1997**, *55*, 13961.

(35) Ahuja, R.; Auluck, S.; Wills, J. M.; Alouani, M.; Johansson, M.; Eriksson, O. *Phys. Rev. B* **1997**, *55*, 4999.

(36) Li, J.-L.; Chun, J.; Wingreen, N. S.; Car, R.; Aksay, I. A.; Saville, D. A. *Phys. Rev. B* **2005**, *71*, 235412.

(37) Hartley, P. A.; Parfitt, G. D. *Langmuir* **1985**, *1*, 651.

(38) Hartley, P. A.; Parfitt, G. D.; Pollack, L. B. *Powder Technol.* **1985**, *42*, 35.

(39) Dagastine, R. R.; Prieve, D. C.; White, L. R. *J. Colloid Interface Sci.* **2002**, *249*, 78.

(40) Parfitt, G. D.; Picton, N. H. *Trans. Faraday Soc.* **1968**, *64*, 1955.